An analytical study of the inductive pattern formation mechanism in Drosophila egg development

C. B. Muratov[(1)] **and S. Y. Shvartsman**[(2)]

[(1)] Department of Mathematical Sciences and
Center for Applied Mathematics and Statistics
New Jersey Institute of Technology, Newark, NJ 07102

[(2)] Department of Chemical Engineering and
Lewis-Sigler Institute for Integrative Genomics
Princeton University, Princeton, NJ 08544

CAMS Report 0203-12, Spring 2003

Center for Applied Mathematics and Statistics

NJIT

An analytical study of the inductive pattern formation mechanism in *Drosophila* egg development

Cyrill B. Muratov* and Stanislav Y. Shvartsman†

*Department of Mathematical Sciences and Center for Applied Mathematics and Statistics, New Jersey Institute of Technology, Newark, NJ 07102

†Department of Chemical Engineering and Lewis-Sigler Institute for Integrative Genomics, Princeton University, Princeton, NJ 08544

Abstract

The complexity and nonlinear dynamics of patterning networks in development make modeling an important approach for the evaluation of the experimentally-derived pattern formation mechanisms. As a rule, models of patterning networks have large numbers of uncertain parameters and model analysis requires extensive computational searches of the parameter space. Analytical techniques can circumvent these difficulties and offer important insights into the networks' functional capabilities. Here, we present an asymptotic analysis of the multiple steady states and transitions between them in a mechanistic model of patterning events specifying the formation of a pair organ in *Drosophila* oogenesis. The model describes the interaction between the spatially nonuniform inductive signal and a network of feedback loops within the layer of epithelial cells. Our approach dramatically reduces the complexity of the problem and provides an explicit analytical method for the construction and parametric analysis of the patterned states responsible for signaling. The analysis reveals a skeleton structure for the patterning capability of the considered regulatory module and demonstrates how a single regulatory network can be used to generate a variety of developmental patterns.

The development of tissues and organs in multicellular organisms is guided by a surprisingly small number of evolutionary conserved regulatory networks [1–3]. It is now becoming apparent that developmental instructions in different species and in different developmental contexts are executed by a set of subroutines, each with a particular developmental function. These subroutines are operated by biomolecular regulatory networks that involve gene expression in individual cells and are integrated by the processes of cell-cell communication. Understanding the functional capabilities of these networks is therefore impossible without studying spatio-temporal dynamics of the underlying signaling patterns.

In systems well characterized by genetics and biochemistry, regulatory mechanisms can be systematically explored via mechanistic modeling and computational analysis (see, for example, [4–7]). Generally, such modeling leads to complicated systems of nonlinear partial differential equations. To gain basic understanding of the underlying patterning mechanisms and predict possible outcomes of genetic manipulations one needs to study, among other things, existence and multiplicity of the stable steady solutions of these equations. These studies are computationally challenging, especially in the presence of a large number of the control parameters. Computational analysis is necessarily limited to particular choices of nonlinearities, parameter sets, etc. Furthermore, interpreting its results may often be difficult because of the presence of "pathological" solutions. In this sense distinguishing the classes of solutions that can be *robustly* realized in a large family of models with certain general properties, as well as the origin of their robustness, is a problem that may lie beyond mere computational studies. This is why direct analytical methods for characterizing these solutions are highly desirable.

Cell communication is crucial in development of multicellular organisms. An important group of cell communication mechanisms relies on regulated release of peptide growth factors [3]. After their release in the extracellular medium, these molecules diffuse to the neighboring cells and activate the cognate receptors on the cell surfaces. The range of signals mediated by secreted growth factors is from one to ~ 10 cells [3, 8]. Recent studies in *Drosophila* have identified a network of growth factors with a rich pattern formation capability. This network includes the Epidermal Growth Factor Receptor (EGFR); signaling through EGFR can activate expression and/or release of its stimulatory and inhibitory ligands, thus forming positive and negative feedback loops [9].

This network is used at many stages of the *Drosophila* development [9,10].

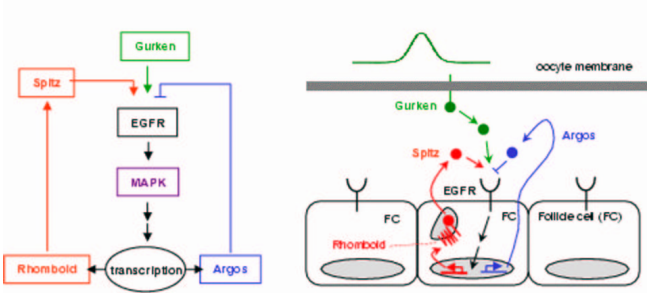

Figure 1: Network connectivity and signaling by autocrine loops in the follicular epithelium in *Drosophila* oogenesis. The oocyte locally secretes a stimulatory ligand Gurken that binds to EGFRs on the surface of follicle cells (FC). EGFR activation in the FC initiates expression of the genes *rhomboid* and *argos*. The corresponding protein product Argos is secreted into the narrow gap between the FC and the oocyte, where it diffuses around and binds to EGFRs, inhibiting their activity. Protein Rhomboid is an intracellular protease that processes an inactive intracellular precursor of Spitz into the biologically active, secreted form. After it is secreted, Spitz diffuses and can then bind to and activate EGFRs on the surfaces of Spits-producing cells and their neighbors.

In oogenesis, it has been proposed to convert the spatially simple, single-peaked signal, into a more complex, two-peaked pattern of signaling activity [11, 12]. Specifically, the layer of identical epithelial cells is locally stimulated by an EGFR ligand. This primary signal is then amplified and expanded by the positive feedback loop that involves the release of a diffusing stimulatory ligand. During this process, an inhibitory ligand is produced, splitting the pattern into two smaller domains of high signaling (for a summary of the signaling network and the identification of the concrete molecular components, see Fig. 1). The resulting pattern with two domains of high receptor activity serves as a blueprint for the development of a pair organ (dorsal appendages) [13, 14].

Interestingly, in other stages of *Drosophila* development the same patterning network generates only single domain signaling patterns from localized inputs [15–17]. A question then arises as to whether the same regulatory network can account for different responses to inductive signals in different developmental contexts. In particular, would extra molecular components be required for establishing different types of signaling patterns (for a discus-

sion, see [11]). To answer these questions, one needs a deeper understanding of the functional capabilities of the regulatory mechanisms involved.

To this end, we take on an analytical approach to the study of signaling patterns in the mechanistic model of a regulatory network in *Drosophila* oogenesis. We perform an asymptotic analysis of the stationary signaling profiles in the model to obtain an analytical characterization of the solutions. Our approach captures the properties of the signaling patterns and allows to investigate their robustness. More importantly, it reveals the core subset of the stationary solutions that are responsible for signaling and demonstrates that their existence and properties do not depend on the details of the model. Our analysis shows that different types of patterns can be obtained in the network of the same topology by varying only a few control parameters.

Model

A mathematical model based on the mechanism of EGFR signaling mediated by positive and negative autocrine feedback loops [11] takes the following form [18]:

$$\frac{\partial S}{\partial t} = D_S \frac{\partial^2 S}{\partial x^2} - k_S S + g_S R, \tag{1}$$

$$\frac{\partial R}{\partial t} = -k_R R + g_R \sigma\{(E - \gamma_R)/\delta_R\}, \tag{2}$$

$$\frac{\partial A}{\partial t} = D_A \frac{\partial^2 A}{\partial x^2} - k_A A + g_A \sigma\{(E - \gamma_A)/\delta_A\}, \tag{3}$$

$$E = S - \alpha A + \beta G. \tag{4}$$

Here, S is the concentration of the stimulatory ligand (the active form of Spitz), G is the concentration of the stimulatory signal (Gurken), A is the concentration of the inhibitory ligand (Argos), all three in the extracellular space; R is the intracellular concentration of the ligand-processing protein (Rhomboid); E is the concentration of the activated EGFRs in the follicle cell membranes (Fig. 1); x is the coordinate along the circumference of the egg, and t is time. The distribution of G serves as a localized inductive signal whose amplitude is ramped up from zero to a steady level at long times. The model involves various rate constants (k's, D's, g's) as well as the sigmoidal nonlinearity $\sigma(x)$ which is characterized by offsets and steepnesses (γ's and δ's, respectively). The level of EGFR activation is positively stimulated by S

and G and is negatively stimulated by A, characterized by constants α and β [18].

Within the framework of the model, the outcome of the patterning events is identified with the stable steady state of the network attained after the transient following the switching on of the inductive signal. Computational analysis of Eqs. (1) – (4) shows that the model can robustly generate complex signaling patterns from simple spatially-distributed inductive signals [18, 19]. Numerical bifurcation studies of the stationary solutions reveal multiple coexisting steady states, whose existence and selection as a function of the control parameters can be correlated with the observed eggshell phenotypes and is in agreement with the large amount of genetic and biochemical data [13].

Asymptotic reduction

Below we develop an asymptotic procedure for analyzing the stationary solutions of Eqs. (1) – (4) in the limit of strong length scale separation between the positive and negative feedback loops. After an appropriate dimensional reduction [18], Eqs. (1) – (4) can be written as

$$\tau_s \frac{\partial s}{\partial t} = \epsilon^2 \frac{\partial^2 s}{\partial x^2} - s + r, \tag{5}$$

$$\tau_a \frac{\partial a}{\partial t} = \frac{\partial^2 a}{\partial x^2} - a + \lambda \sigma\{(s - a + g - c_a)/b_a\}, \tag{6}$$

$$\frac{\partial r}{\partial t} = -r + \sigma\{(s - a + g - c_r)/b_r\}, \tag{7}$$

$$g(x,t) = g_0(t) \exp(-x^2/x_0^2), \quad \sigma(x) = \frac{x^2 \theta(x)}{1 + x^2}, \tag{8}$$

where s, a, r, g are the dimensionless concentrations and $\theta(x)$ is the Heaviside function. For concreteness we assumed a particular form of the dependence of g on x and a particular form of the sigmoidal function $\sigma(x)$. Functionally, s is a short-ranged *messenger*, r is an autocrine *switch*, a is the long-ranged *inhibitor*, and g is the localized stimulating inductive signal [18]. Since the experimentally observed patterns are highly localized [20, 21], the no flux boundary conditions for Eqs. (5) and (6) can be pushed off to infinity.

Thus, the qualitative properties of the solutions are determined by a number of dimensionless parameters: $c_{r,a}$ are the dimensionless offsets and $b_{r,a}$ are the dimensionless steepnesses of the sigmoidal functions in the production

of r and a, respectively; λ is the relative strength of the negative feedback; $g_0(t)$ and x_0 characterize the amplitude and width of the time-dependent inductive signal; $\tau_{s,a}$ are the time scales of s and a relative to that of r, and ϵ is the ratio of the length scales of s and a. The available biochemical information suggests that the latter is a small parameter: $\epsilon \simeq 0.1$, while $x_0 \simeq 3$ [11,20,22]. Therefore, we will take advantage of this fact and construct the solutions of Eqs. (5) – (7) in the limit $\epsilon \to 0$. We are also going to make another simplifying assumption supported by the experiments that the response of a to the activation of EGFR is characterized by a sharp threshold higher than that of r [11, 17, 21, 23]. In the model, this translates to taking the limit $b_a \to 0$, thus replacing the sigmoidal function in Eq. (6) with the Heaviside step, and assuming that $c_a > c_r$.

Numerical simulations of Eqs. (5) – (8) show that for sufficiently slowly varying signal amplitudes $g_0(t)$ the dynamics are governed by a series of abrupt transitions between different types of quasistationary signaling patterns [18]. To illustrate this, we show a simulation in which $g_0(t)$ is slowly ramped up from zero to a certain level and then decreased back to zero in the same fashion (Fig. 2). One can see a sequence of transitions from no signaling (0 pulses) $\to$ 1 narrow pulse $\to$ 2 pulses $\to$ 1 broad pulse when g_0 is increased. Similarly, upon decreasing g_0 the 1 broad pulse solution transforms into 2 pulses, which then disappear at a critically low level of inductive signal. Note the hysteretic character of the transitions.

The nature of large-amplitude patterns in the model

For similar systems of reaction-diffusion equations *without* any inductive signals it is well established that for $\epsilon \ll 1$ stable large amplitude stationary solutions have the form of domains separated by narrow domain walls (see, for example [24–27]). This is also what we see as outcomes of the transitions triggered by the adiabatic variation of the inductive signal (see Fig. 2). Therefore, in the following we will be looking for the solutions of this type. In the limit $\epsilon \to 0$ these stationary solutions break up into the inner and outer solutions, which vary on the length scales of ϵ and 1, respectively (see also [24–30]). Let us introduce a slowly varying quantity

$$v(x) = a(x) - g(x) + c_r. \tag{9}$$

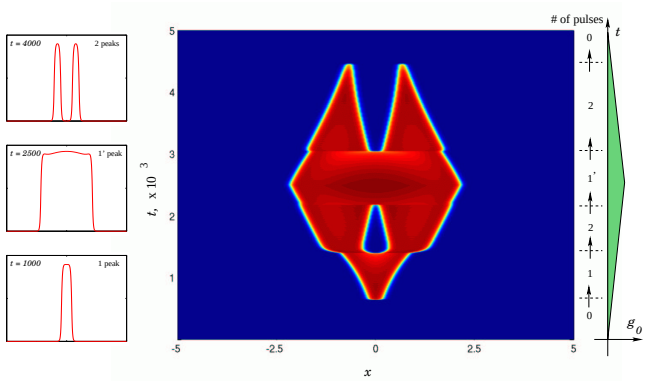

Figure 2: A sequence of transitions and the hysteresis by adiabatically varying inductive signal. The snapshots of the distributions of s at different times are shown on the left. The color-coded space-time plot of the distribution of s is shown in the center, with "red" corresponding to $s \simeq 1$ and "blue" corresponding to $s \simeq 0$. Results of the numerical solutions of Eqs. (5) – (8) with $\epsilon = 0.05$, $\lambda = 1.6$, $c_a = 0.5$, $b_a = 0.05$, $c_r = 0.4$, $b_r = 0.2$, $x_0 = 3$, $\tau_s = 0.1$, $\tau_a = 1$. The signal amplitude is taken to be $g_0(t) = 1.6 \times t/2500$ for $0 \le t \le 2500$ and $g_0(t) = 1.6 \times (2 - t/2500)$ for $2500 \le t \le 5000$ (right).

Then, on the inner scale we can assume that $v(x) \simeq v_0 = \text{const}$, so the stationary Eqs. (5) and (7) for the inner solution become

$$0 = \epsilon^2 s_{xx} + f(s, v_0), \quad f(s, v_0) = -s + \sigma\left\{\frac{s - v_0}{b_r}\right\}. \tag{10}$$

It is easy to see that for small enough b_r ($b_r < 0.6086$ for our choice of σ) the nonlinearity $f(s)$ is N-shaped, so equation $f(s, v_0) = 0$ has three roots: $s_-(v_0) < s_0(v_0) < s_+(v_0)$, whenever $v_{\min} < v_0 < v_{\max}$. Furthermore, when v_0 satisfies

$$\int_{s_-(v_0)}^{s_+(v_0)} f(s, v_0) ds = 0, \tag{11}$$

Eq. (10) has solutions in the form of the domain walls connecting $s_-(v_0)$ with $s_+(v_0)$ [24–26, 29, 30]. The quantities above can be easily calculated numerically for any fixed value of b_r. For example, for $b_r = 0.2$, we find that $v_0 \simeq 0.2398$, $v_{\max} \simeq 0.4042$ and $v_{\min} \simeq -0.0101$.

On the outer scale the derivative term in Eq. (5) can be neglected, so s obeys the local coupling relation $s = s_\pm(v)$, where $s_+(v)$ and $s_-(v)$ are

the smallest and the largest roots of equation $f(s,v)=0$ corresponding to the "on" and "off" states of the positive feedback, respectively, with $s_+(v)$ defined for $v \le v_{\max}$ and $s_-(v)$ defined for $v \ge v_{\min}$. Furthermore, for c_a not much larger than c_r and $b_a \to 0$ the distribution of a satisfies Eq. (6), in which the sigmoidal function is replaced by the characteristic function of the "on" state. If the i-th "on" domain, which we will call a *pulse*, is characterized by the position of its center r_i and width w_i, then it is not difficult to show that the solution of Eq. (6) inside the i-th pulse is

$$a(x) = \lambda\Big[\sum_{i\neq j} \sinh\frac{w_j}{2} e^{-|x-r_j|} + 1 - e^{-\frac{w_i}{2}}\cosh(x-r_i)\Big], \tag{12}$$

while outside all the pulses it is given by

$$a(x) = \lambda \sum_j \sinh\frac{w_j}{2} e^{-|x-r_j|}. \tag{13}$$

Matching the outer and inner solutions at the boundaries of the pulses, we obtain the self-consistency condition

$$v(r_i \pm w_i/2) = v_0. \tag{14}$$

This equation, together with Eq. (12), determines the positions and widths of each pulse in a stationary pattern with an arbitrary number of pulses. Note that the sigmoidal nonlinearity in the positive feedback now enters the problem only through the values of v_0, $v_{\min}$ and $v_{\max}$.

State of no signaling

When the system is in the "off" state, we have $a=0$, so from Eq. (9) we see that such a solution exists as long as $v = -g(x) + c_r \ge v_{\min}$. If the value of g_0 is increased, the first point at which this condition gets violated is $x=0$, so when $g_0 = g_0^{(0\to 1)} = c_r - v_{\min}$, the all "off" solution disappears. Dynamically, this corresponds to switching of the positive feedback on at $x=0$ and leads to a transition from zero to one pulse ("ignition") (Fig. 2). Let us point out that in our model a Turing-like instability is never realized even for very broad inductive signals, since the positive feedback is switched on at the level of EGFR activity at which the diffusive inhibitor is not produced.

Therefore, in our model signaling patterns can develop only through a series of abrupt transitions between large-amplitude *localized* patterns. See [18] for more discussion of the distinctions with the classical activator-inhibitor mechanism [24,31–33]. Let us emphasize that in our model pattern formation scenarios are governed by the interplay between long-range inhibition and strong localized stimulation by an inductive signal.

Single pulse solution

Most of the properties of the signaling patterns forming in the model can be inferred from the analysis of the simplest inhomogeneous pattern: a single pulse. These patterns, also called *autosolitons*, play a fundamental role in systems with competing positive and negative feedbacks [24]. For this reason, in this paper we will mostly concentrate on the construction and properties of the one pulse solution. More complex inhomogeneous patterns, as well as their stability and dynamics will be studied elsewhere.

Existence

Since for a single pulse the function $a(x)$ given by Eq. (12) is symmetric relative to its center, Eq. (14) can only be satisfied when $r_1 = 0$. Substituting this into Eqs. (9), (12), and (14), after a simple calculation we obtain that the pulse of width w_1 exists when $g_0 = g_0^{(1)}$, where

$$g_0^{(1)} = \left(\frac{\lambda}{2}(1 - e^{-w_1}) + c_r - v_0\right) e^{w_1^2/4x_0^2}. \tag{15}$$

By inspection, this is a monotonically increasing function of w_1, so for each large enough value of g_0 there is a *unique* one pulse solution. An example of such a solution is shown in Fig. 3(a).

In the model, the value of c_r is chosen to be greater than v_0, so that the one pulse solutions do not exist in the absence of the inductive signal, consistent with the experimental data [34]. Therefore, since $w_1 > 0$, we must have $g_0 > g_0^{(1\to 0)} = c_r - v_0$ for the solution to exist. Dynamically, the one pulse solution collapses when g_0 is slowly decreased below $g_0^{(1\to 0)}$ ("extinction") [18]. Thus, for $g_0^{(1\to 0)} \le g_0 \le g_0^{(0\to 1)}$ there is coexistence of zero and one pulse solutions.

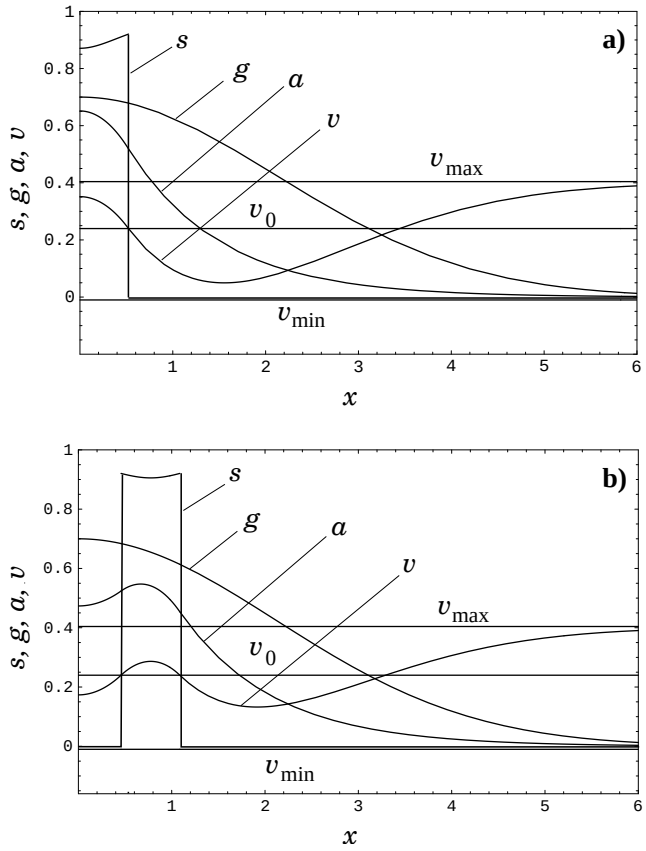

Figure 3: Asymptotic one and two pulse solutions (only half of the solution is shown). The parameters are: $b_r = 0.2$, $c_r = 0.4$, $\lambda = 1.6$, $g_0 = 0.7$, $x_0 = 3$.

Splitting

The regions of existence of the one pulse solutions are limited by the possibility of the *local breakdown* in the center or the tails of the pulse (for general reaction-diffusion systems see, for example, [24, 35–40]). In our model the local breakdown will occur in the center of the pulse when the value of v reaches $v_{\max}$ at $x = 0$ (see Fig. 3), making the value of s jump down to the lower branch of the local coupling curve $s_{\pm}(v)$. Using Eq. (12) to calculate $v(0)$ and combining it with Eq. (15), after a simple calculation we obtain that the local breakdown in the pulse center occurs when $x_0 > x_0^{(1\to 2)}$, with

$$x_0^{(1\to 2)} = \frac{w_1}{2} \ln^{-1/2} \left[\frac{\lambda(1 - e^{-w_1/2}) + c_r - v_{\max}}{\frac{1}{2}\lambda(1 - e^{-w_1}) + c_r - v_0} \right]. \tag{16}$$

This equation, together with Eq. (15), determines parametrically the boundary of existence of the one pulse solution due to the local breakdown in the center. Dynamically, upon crossing this boundary the positive feedback switches off in the center of the pulse, so one pulse solution splits into two pulses (Fig. 2).

Ignition in the tail

Alternatively, the value of v can reach $v_{\min}$ somewhere outside the pulse (see Fig. 3). This will occur first at the point x at which v reaches a minimum, so, using Eq. (13) to calculate v, we obtain a system of transcendental equations:

$$v_{\min} = \lambda \sinh \frac{w_1}{2} e^{-x} - g_0 e^{-x^2/x_0^2} + c_r, \tag{17}$$

$$0 = -\lambda \sinh \frac{w_1}{2} e^{-x} + \frac{2g_0 x}{x_0^2} e^{-x^2/x_0^2} \tag{18}$$

These equations, together with Eq. (15), are solved numerically to find the value of $x_0 = x_0^{(1\to 3)}$ as a function of g_0 at which the one pulse solution disappears. Once again, dynamically this results in the ignition of a pair of pulses in the tails of the one pulse solution and thus leads to a transition from one to three pulses [18, 19].

Two pulse solution

Let us now consider a symmetric ($r_2 = -r_1$, $w_2 = w_1$) two pulse solution which corresponds to the established signaling pattern in the wild type phe-

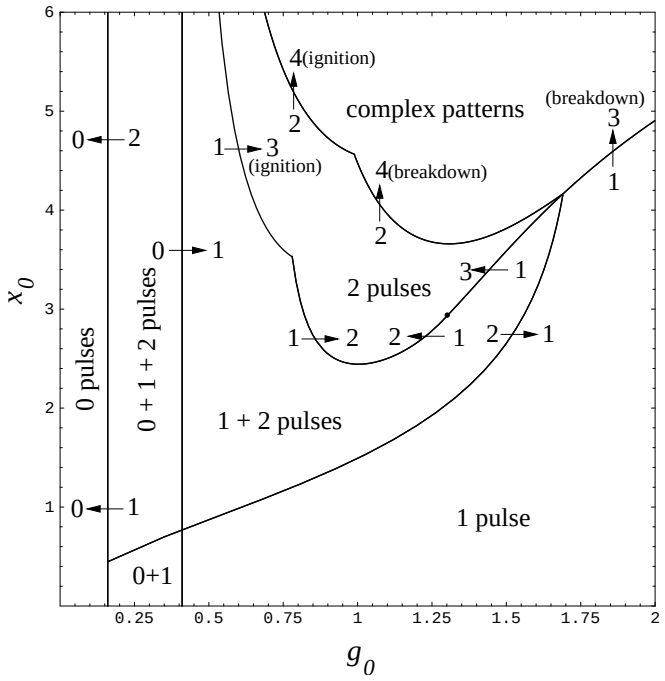

Figure 4: Multiple steady states and transitions between them as functions of the inductive signal's width and amplitude. The network parameters are: $b_r = 0.2$, $c_r = 0.4$, $\lambda = 1.6$.

notype [11]. A long but straightforward calculation from Eqs. (12) and (14) shows that a solution with the given values of r_1 and w_1 exists when $g_0 = g_0^{(2)}$ and $x_0 = x_0^{(2)}$, where

$$x_0^{(2)} = \frac{\sqrt{2r_1 w_1}}{\ln^{1/2}\left(\frac{c_r - v_0 + \frac{\lambda}{2}\left(1-e^{-w_1}\right) + \frac{\lambda}{2}(e^{w_1}-1)e^{-2r_1}}{c_r - v_0 + \frac{\lambda}{2}\left(1-e^{-w_1}\right) + \frac{\lambda}{2}\left(1-e^{-w_1}\right)e^{-2r_1}}\right)}, \tag{19}$$

$$g_0^{(2)} = \left(\frac{c_r - v_0 + \frac{\lambda}{2}\left(1-e^{-w_1}\right) + \frac{\lambda}{2}\left(e^{w_1}-1\right)e^{-2r_1}}{c_r - v_0 + \frac{\lambda}{2}\left(1-e^{-w_1}\right) + \frac{\lambda}{2}\left(1-e^{-w_1}\right)e^{-2r_1}}\right)^{\frac{(2r_1-w_1)^2}{8w_1 r_1}} \times \left(c_r - v_0 + \frac{\lambda}{2}\left(1+e^{w_1-2r_1}\right)\left(1-e^{-w_1}\right)\right). \tag{20}$$

In general, existence and multiplicity of the two pulse solutions can be studied graphically by looking at the level sets generated by these equations. We find that for a wide range of the parameters there is a unique symmetric two pulse solution for a given inductive signal. An example of such a solution is shown in Fig. 3(b).

Equations (19) and (20) allow to determine two boundaries of existence for the two pulse solutions in the parameter space. One corresponds to disappearance of solutions as both r_1 and w_1 go to zero. According to these equations, this can happen for any x_0, when g_0 approaches $g_0^{(2\to 0)} = g_0^{(1\to 0)} = c_r - v_0$. The other comes from the geometric constrain that $r_1 > w_1/2$, crossing this boundary corresponds to merging of pulses into a single broad pulse (Fig. 2). Substituting $r_1 = w_1/2$ into Eq. (19), we find the value of $x_0 = x_0^{(2\to 1)}$ at which the two pulse solution disappears:

$$x_0^{(2\to 1)} = w_1 \ln^{-1/2}\left[\frac{c_r - v_0 + \lambda(1-e^{-w_1})}{c_r - v_0 + \frac{1}{2}\lambda(1-e^{-2w_1})}\right]. \tag{21}$$

It is also possible to study boundaries of existence of the two pulse solutions associated with the local breakdown and ignition in the tails in the way similar to that for a single pulse.

Multiparametric analysis

The analytical expressions for the boundaries of existence of different types of stationary solutions obtained above can be easily used to perform multi-

parametric studies in *all* of the parameters involved in the asymptotic formulation. Let us, for example, show a two-parameter "cut" through the parameter space, corresponding to the fixed network parameters (Fig. 4). This diagram shows regions of existence of zero, one, and two pulse solutions as functions of the inductive signal, and transitions between them. In this figure, we also showed the boundaries of existence of one and two pulse solutions associated with more complex transitions.

The diagram in Fig. 4 can be conveniently used to quantify signaling patterns for different network parameters. We find that variations in the threshold c_r or steepness b_r of the positive feedback, or the strength of negative feedback λ do not change significantly the structure of Fig. 4, they basically stretch or shift it around in the $g_0 - x_0$ plane. This demonstrates robustness of the considered patterning network with respect to variations of the network parameters. On the other hand, we found that the structure of the diagram in Fig. 4 is strongly affected by the *shape* of the sigmoidal nonlinearity σ, expressed in the relationship between $v_{\min}$, v_0, and $v_{\max}$. Changing the location of v_0 relative to $v_{\max}$ and $v_{\min}$ results in the relative motion of the $1 \to 2$ and the $1 \to 3$ transition curves. It turns out that in order for the transition $1 \to 2$ to occur before the $1 \to 3$ transition, the value of v_0 must be shifted closer to $v_{\max}$. This requires a substantial degree of asymmetry between the "on" and "off" states of the positive feedback loop. Note that such an insight must be very difficult to obtain in merely computational studies.

Let us summarize the results of our asymptotic analysis of the stationary signaling patterns (see Fig. 4). First, there are large regions of the parameter space where the inhomogeneous patterns including those consisting of one and two pulses *exist*. Second, the regions of existence of different types of stationary patterns overlap, so for certain values of the parameters different patterns may *coexist*. Third, crossing the boundaries of existence of a pattern results in an abrupt *transition* to a different kind of pattern; these transitions will govern selection of the outcome. Thus, the formation of a two-peaked signaling pattern in *Drosophila* oogenesis may be viewed as a sequence of *transitions* from zero to one to two pulses driven by a slow increase of the inductive signal's amplitude as the egg develops, Fig. 5(a).

For comparison, let us examine the one-parameter bifurcation cuts together with transitions between the quasistationary patterns obtained computationally for the same network and inductive signal parameters, but different values of ϵ. At $\epsilon = 0.05$ the diagram in Fig. 5(d) essentially coincides

with the asymptotics [Fig. 5(a)]. When the value of ϵ is increased [Figs. 5(c),(b)], the overall structure of the transitions remains; however, a number of deviations may be observed. First, for small values of g_0 the amplitude of the one pulse solution becomes very small, down to 10% at the threshold. Second, the transition between two pulse solution and the one broad pulse solution splits into a sequence of two transitions, with a new two pulse solution appearing in a very narrow region of the parameters. This solution has two peaks, however the level of signaling remains relatively high in the center of the pattern. Let us emphasize that at the present level of modeling these solutions cannot be reliably identified with the underlying signaling patterns in *Drosophila* oogenesis and may be artifacts of the model.

Finally, our analysis indicates that there exists a large region in the parameter space in which two pulse solutions exist while single pulse solutions do not (see Fig. 4). This feature of the asymptotic limit persists in the full model [18]. In this region a simple one-peaked inductive signal must necessarily result in complex spatial response. We believe that this is a robust feature of the considered patterning mechanism and is at the heart of the induction of a pair organ by a simple single-peaked input.

Discussion

In conclusion, we have performed an asymptotic analysis of the large-amplitude solutions in a mathematical model of a spatially distributed patterning network in *Drosophila* oogenesis. Our method allows a very efficient way of constructing strongly nonlinear solutions, characterizing the domains of their existence, and interpreting the dynamics of the patterns. Furthermore, it reveals the core subset of the stationary solutions which provide the skeleton structure for the considered patterning mechanism. We have verified that the obtained solutions are in fact good approximations for the solutions of the full model. Moreover, our approach allows to guide computational studies of patterning mechanisms by quickly identifying the parameter regions of interest and then focusing on them in the large-scale computational analysis.

The fact that the one pulse solutions cease to exist for a wide range of single-peaked inductive signals is a striking result. It means that in this range single peaked signals will always be converted into complex patterns. Let us emphasize that signaling patterns in development are biological blueprints, so this patterning capability might be employed in the mechanisms leading

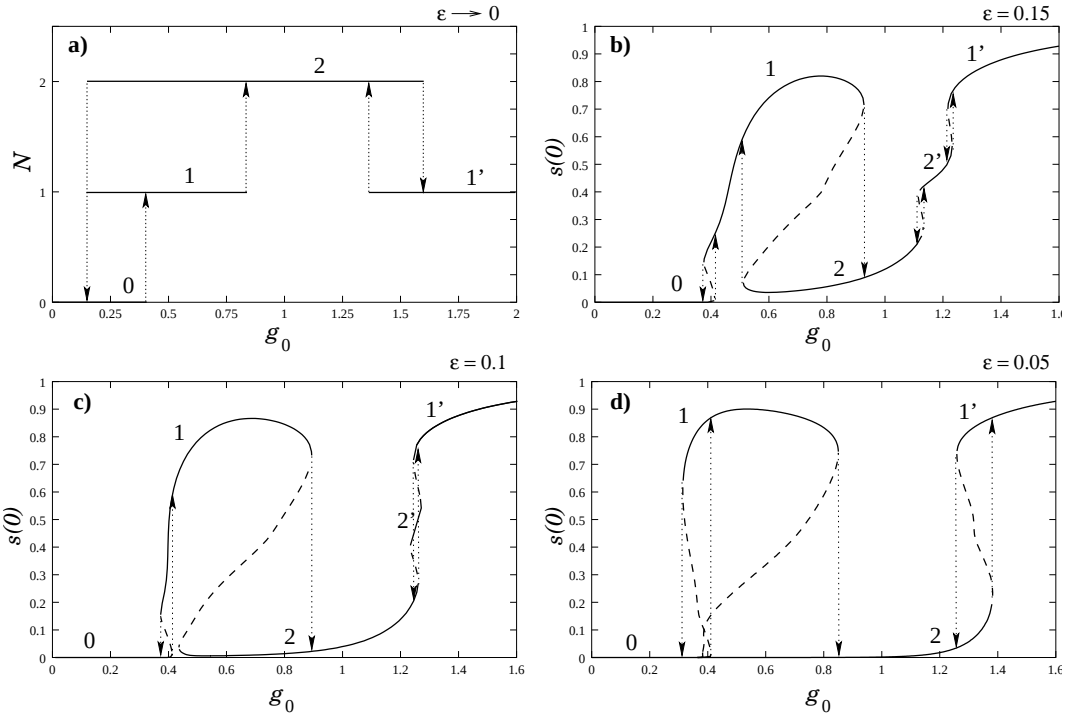

Figure 5: (a) The sequence of transitions upon the adiabatic variation of the inductive signal's amplitude. (b) – (d) One parameter bifurcation cuts showing the value of s in the center of the system in the stationary solutions of the full model and transitions between them [Eqs. (5) – (8)]. The parameters are as in Fig. 2, except $\epsilon = 0.15$ (b), $\epsilon = 0.1$ (b), and $\epsilon = 0.05$ (d). N in (a) is the number of pulses; numbers in (b) – (d) indicate different stationary solutions with the corresponding number of peaks, solid lines show stable, and dashed lines — unstable solutions.

to complex tissue morphologies in a number of developmental contexts [2,11].

The existence of multiple steady states of the signaling network suggests versatility of the considered patterning mechanism. Hence, the irreversible commitment mechanism does not have to be invoked in order to explain why inhibition by Argos generates single-domain signaling patterns in other stages of fruit fly development (compare with [11]). Furthermore, the mechanism robustly predicts the existence of patterns with more than two domains of high signaling, suggesting a possibility of more complex eggshell phenotypes. Such phenotypes can indeed be generated by genetic manipulations of the patterning network [41, 42]. They are also observed in the wild type phenotypes of the related fly species [20, 43].

Our method provides a direct way of assessing robustness of the patterning mechanism by giving explicit analytical criteria for the existence of the stationary solutions. Moreover, it allows reformulation of the problem of existence in terms of the parameters of the solutions (like the width of the pulses and the distance between them for the two pulse solution, for example) rather than in terms of the control parameters. Thus, it allows to solve the inverse problem of finding appropriate parameter ranges and nonlinearities in order for a specified type of a signaling pattern to be realized.

Our asymptotic technique allows a number of natural extensions. It is possible to generalize our analysis to higher-dimensional stationary patterns in the presence of multiple inhomogeneous inductive signals. There is a number of experimental and computational indications that this extension is necessary and relevant to the real patterning module [12, 18, 19]. In another direction, the analysis of the stationary patterns can be generalized to patterns in the form of moving pulses (for similar approaches, see [38, 44–48]). In this description, pulses will be created or destroyed as a result of the local breakdown. This hybrid kinematic description will allow to assess stability and selection of the outcomes of patterning events and may provide a way to probe the optimal dynamical strategies for inductive signal design necessary for selecting a particular pattern out of the multitude of possible ones.

This work was supported by the National Science Foundation Grant DMS-0211864.

References

[1] Wolpert, L., Beddington, R., Jessel, T., Lawrence, P., & Meyerowitz, E. (1998) *Principles of Development* (Oxford University Press, Oxford).

[2] Hogan, B. L. M. (1999) *Cell* **96**, 225–233.

[3] Freeman, M. & Gurdon, J. B. (2002) *Annu. Rev. Cell Dev. Biol.* **18**, 515–539.

[4] Palsson, E., Lee, K. J., Goldstein, R. E., Franke, J., Kessin, R. H., & Cox, E. C. (1997) *Proc. Natl. Acad. Sci. USA* **94**, 13719–13723.

[5] Reinitz, J., Kosman, D., Vanario-Alonso, C. E., & Sharp, D. H. (1998) *Dev. Genet.* **23**, 11–27.

[6] von Dassow, G., Meir, E., Munro, E. M., & Odell, G. M. (2000) *Nature* **406**, 188–192.

[7] Yuh, C. H., Bolouri, H., & Davidson, E. H. (1998) *Science* **279**, 1896–1902.

[8] Hatini, V. & Di Nardo, S. (2001) *Trends Genet.* **17**, 574–579.

[9] Casci, T. & Freeman, M. (1999) *Cancer Metast. Rev.* **18**, 181–201.

[10] Van Buskirk, C. & Schupbach, T. (1999) *Trends Cell Biol.* **9**, 1–4.

[11] Wasserman, J. D. & Freeman, M. (1998) *Cell* **95**, 355–364.

[12] Barkai, N. & Shilo, B.-Z. (2002) *Curr. Biol.* **12**, R493–R495.

[13] Nilson, L. A. & Schupbach, T. (1999) *Curr. Top. Dev. Biol.* **44**, 203–243.

[14] Dobens, L. L. & Raftery, L. A. (2000) *Dev. Dynam.* **218**, 80–93.

[15] Freeman, M. (1997) *Development* **124**, 261–270.

[16] Stemerdink, C. & Jacobs, J. R. (1997) *Development* **124**, 3787–3796.

[17] Golembo, M., Schweitzer, R., Freeman, M., & Shilo, B. Z. (1996) *Development* **122**, 223–230.

[18] Shvartsman, S. Y., Muratov, C. B., & Lauffenburger, D. A. (2002) *Development* **129**, 2577–2589.

[19] Přibyl, M., Muratov, C. B., & Shvartsman, S. Y. (2003) *Dev. Dynam.* **226**, 155–159.

[20] Peri, F., Bokel, C., & Roth, S. (1999) *Mech. Dev.* **81**, 75–88.

[21] Queenan, A. M., Ghabrial, A., & Schupbach, T. (1997) *Development* **124**, 3871–3880.

[22] Stevens, L. (1998) *Cell* **95**, 291–294.

[23] Schweitzer, R., Howes, R., Smith, R., Shilo, B. Z., & Freeman, M. (1995) *Nature* **376**, 699–702.

[24] Kerner, B. S. & Osipov, V. V. (1994) *Autosolitons: a New Approach to Problems of Self-Organization and Turbulence* (Kluwer, Dordrecht).

[25] Kerner, B. S. & Osipov, V. V. (1980) *Sov. Phys. – JETP* **52**, 1122–1132.

[26] Mimura, M., Tabata, M., & Hosono, Y. (1980) *SIAM J. Math. Anal.* **11**, 613–631.

[27] Nishiura, Y. & Fujii, H. (1987) *SIAM J. Math. Anal.* **18**, 1726–1770.

[28] Ortoleva, P. & Ross, J. (1975) *J. Chem. Phys.* **63**, 3398–3408.

[29] Fife, P. C. (1976) *J. Math. Anal. Appl.* **54**, 497–521.

[30] Vasileva, A. B., Butuzov, V. F., & Kalachev, L. V. (1995) *The Boundary Function Method for Singular Perturbation Problems* (SIAM, Philadelphia).

[31] Turing, A. M. (1952) *Phil. Trans. R. Soc. London B* **237**, 37–72.

[32] Mikhailov, A. S. (1990) *Foundations of Synergetics* (Springer-Verlag, Berlin).

[33] Gierer, A. & Meinhardt, H. (1972) *Kybernetik* **12**, 30–39.

[34] Guichet, A., Peri, F., & Roth, S. (2001) *Dev. Biol.* **237**, 93–106.

[35] Kerner, B. S. & Osipov, V. V. (1982) *Sov. Phys. – Doklady* **27**, 484–486.

[36] Gafiichuk, V. V., Kerner, B. S., Osipov, V. V., & Yuzhanin, A. G. (1990) *Zh. Tekh. Fiz.* **60**, 8–13.

[37] Reynolds, W. N., Pearson, J. E., & Ponce-Dawson, S. (1994) *Phys. Rev. Lett.* **72**, 2797–2800.

[38] Reynolds, W. N., Ponce-Dawson, S., & Pearson, J. E. (1997) *Phys. Rev. E* **56**, 185–198.

[39] Nishiura, Y. & Ueyama, D. (1999) *Physica D* **130**, 73–104.

[40] Muratov, C. B. & Osipov, V. V. (2000) *J. Phys. A: Mat. Gen.* **33**, 8893–8916.

[41] Reich, A., Sapir, A., & Shilo, B. Z. (1999) *Development* **126**, 4139–4147.

[42] Deng, W. M. & Bownes, M. (1997) *Development* **124**, 4639–4647.

[43] Hinton, H. E. (1981) *Biology of Insect Eggs* (Pergamon Press, Oxford; New York), Vol 1.

[44] Nishiura, Y. & Mimura, M. (1989) *SIAM J. Appl. Math.* **49**, 481–514.

[45] Ohta, T., Ito, A., & Tetsuka, A. (1990) *Phys. Rev. A* **42**, 3225–3232.

[46] Muratov, C. B. (1997) *Phys. Rev. E* **55**, 1463–1477.

[47] Doelman, A., Eckhaus, W., & Kaper, T. J. (2001) *SIAM J. Appl. Math.* **61**, 2036–2062.

[48] Iron, D. & Ward, M. J. (2002) *SIAM J. Appl. Math.* **62**, 1924–1951.